The Apparently Decaying Orbit of WASP-12b

The Astronomical Journal, 154:4 (10pp), 2017 July https://doi.org/10.3847/1538-3881/aa6d75

The Apparently Decaying Orbit of WASP-12b

Kishore C. Patra[1], Joshua N. Winn[2], Matthew J. Holman[3], Liang Yu[1], Drake Deming[4], and Fei Dai[1,2]
[1] Department of Physics, and Kavli Institute for Astrophysics and Space Research, Massachusetts Institute of Technology, Cambridge, MA 02139, USA
[2] Department of Astrophysical Sciences, Princeton University, 4 Ivy Lane, Princeton, NJ 08540, USA
[3] Harvard-Smithsonian Center for Astrophysics, 60 Garden Street, Cambridge, MA 02138, USA
[4] Department of Astronomy, University of Maryland at College Park, College Park, MD 20742, USA
Received 2017 March 19; revised 2017 April 13; accepted 2017 April 14; published 2017 June 9

Abstract

We present new transit and occultation times for the hot Jupiter WASP-12b. The data are compatible with a constant period derivative: $\dot{P} = -29 \pm 3$ ms yr^{-1} and $P/\dot{P} = 3.2$ Myr. However, it is difficult to tell whether we have observed orbital decay or a portion of a 14-year apsidal precession cycle. If interpreted as decay, the star's tidal quality parameter $Q_\star$ is about 2×10^5. If interpreted as precession, the planet's Love number is 0.44 ± 0.10. Orbital decay appears to be the more parsimonious model: it is favored by $\Delta\chi^2 = 5.5$ despite having two fewer free parameters than the precession model. The decay model implies that WASP-12 was discovered within the final $\sim$0.2% of its existence, which is an unlikely coincidence but harmonizes with independent evidence that the planet is nearing disruption. Precession does not invoke any temporal coincidence, but it does require some mechanism to maintain an eccentricity of $\approx$0.002 in the face of rapid tidal circularization. To distinguish unequivocally between decay and precession will probably require a few more years of monitoring. Particularly helpful will be occultation timing in 2019 and thereafter.

Key words: planet–star interactions – planets and satellites: individual (WASP-12 b)

1. Introduction

More than 20 years have elapsed since the discovery of hot Jupiters (Mayor & Queloz 1995). The time may be ripe to confirm a long-standing theoretical prediction: the orbits of almost all of these planets should be shrinking due to tidal orbital decay (Rasio et al. 1996; Sasselov 2003; Levrard et al. 2009). This is because the star's rotational angular momentum is typically smaller than one-third of the orbital angular momentum, the critical value beneath which tidal evolution has no stable equilibrium (Hut 1980).

Tidal decay of hot Jupiters has been invoked to explain certain properties of the ensemble of star-planet systems. For example, the scarcity of gas giants with periods less than a day is suggestive of orbital decay (see, e.g., Jackson et al. 2008; Hansen 2010; Penev et al. 2012; Ogilvie 2014). The anomalously rapid rotation of some hot-Jupiter host stars has been attributed to transfer of the planet's orbital angular momentum (Penev et al. 2016). The absence of hot Jupiters around subgiant stars may be caused by an acceleration of orbital decay when a star leaves the main sequence (Villaver & Livio 2009; Hansen 2010; Schlaufman & Winn 2013). Tidal decay might also be responsible for the lower occurrence of close-in planets around rapidly rotating stars (Teitler & Königl 2014) or the realignment of stars and their planetary orbits (Matsakos & Königl 2015). However, direct evidence for orbital decay has been lacking: there have been no clear demonstrations of a long-term period decrease due to orbital decay (see, e.g., Hoyer et al. 2016; Wilkins et al. 2017).

Another unfulfilled prediction is that the orbits of hot Jupiters should be apsidally precessing on a timescale of decades (Miralda-Escudé 2002; Heyl & Gladman 2007; Jordán & Bakos 2008; Pál & Kocsis 2008), as long as the orbits are at least slightly eccentric. In particular, Ragozzine & Wolf (2009) noted that the theoretical precession rate is dominated by the contribution from the planet's tidally deformed mass distribution. They advocated a search for apsidal precession as a means of probing the interiors of hot Jupiters.

With an orbital period of 1.09 days, WASP-12b is one of the shortest-period giant planets known (Hebb et al. 2009) and has been monitored for a decade. It is, therefore, an outstanding target in the search for orbital decay and apsidal precession. Maciejewski et al. (2016) reported a decrease in the apparent period. Despite being the most convincing claim that has yet been presented for orbital decay, those authors could not distinguish between true period shrinkage and a long-term oscillation of the apparent period due to apsidal precession. In this paper, we present new transit and occultation times (Sections 2 and 3). We use all of the available data to test which model is favored by the data: a constant period derivative or sinusoidal variations arising from apsidal precession (Section 4). We also discuss the implications of both models (Section 5) and prospects for future observations (Section 6).

2. New Transit Times

Between 2016 October and 2017 February, we observed seven transits of WASP-12 with the 1.2 m telescope at the Fred Lawrence Whipple Observatory on Mt. Hopkins, Arizona. Images were obtained with the KeplerCam detector through a Sloan r'-band filter. The typical exposure time was 15 s, chosen to give a signal-to-noise ratio of about 200 for WASP-12. The field of view of this camera is $23'.1$ on a side. We used 2×2 binning, giving a pixel scale of $0''.68$.

The raw images were processed by performing standard overscan correction, debiasing, and flat-fielding with IRAF.[5] Aperture photometry was performed for WASP-12 and an ensemble of 7–9 comparison stars of similar brightness. The

[5] The Image Reduction and Analysis Facility (IRAF) is distributed by the National Optical Astronomy Observatory, which is operated by the Association of Universities for Research in Astronomy (AURA) under a cooperative agreement with the National Science Foundation.

aperture radius was chosen to give the smallest scatter in the flux outside of the transits and was generally 7–8 pixels. The reference signal was generated by summing the flux of the comparison stars. The flux of WASP-12 was then divided by this reference signal to produce a time series of relative flux. Each time series was normalized to have unit flux outside of the transit. The time stamps were placed on the BJD_{TDB} system using the code of Eastman et al. (2010).

We fitted a Mandel & Agol (2002) model to the data from each transit. The parameters of the transit model were the midtransit time, the planet-to-star radius ratio ($R_p/R_\star$), the scaled stellar radius ($R_\star/a$), and the impact parameter ($b = a\cos i/R_\star$). For given values of $R_\star/a$ and b, the transit timescale is proportional to the orbital period (see, e.g., Equation (19) of Winn 2010). To set this timescale, we held the period fixed at 1.09142 days, although the individual transits were fitted separately with no requirement for periodicity. To correct for differential extinction, we allowed the apparent magnitude to be a linear function of airmass, giving two additional parameters. The limb darkening law was assumed to be quadratic, with coefficients held fixed at the values ($u_1 = 0.32$, $u_2 = 0.32$) tabulated by Claret & Bloemen (2011) for a star with the spectroscopic parameters given by Hebb et al. (2009).[6]

To determine the credible intervals for the parameters, we used the *emcee* Markov Chain Monte Carlo (MCMC) code written by Foreman-Mackey et al. (2013). The transition distribution was proportional to $\exp(-\chi^2/2)$ with

$$\chi^2 = \sum_{i=1}^{N}\left(\frac{f_{\mathrm{obs},i} - f_{\mathrm{calc},i}}{\sigma_i}\right)^2, \quad (1)$$

where $f_{\mathrm{obs},i}$ is the observed flux at time t_i and $f_{\mathrm{calc},i}$ is the corresponding flux of the model. The uncertainties σ_i were set equal to the standard deviation of the out-of-transit data. In a few cases, the pre-ingress scatter was noticeably different than the post-egress scatter; for those observations, we assigned σ_i by linear interpolation between the pre-ingress and post-egress values.

Figure 1 shows the light curves and the best-fit models. Table 1 reports the midtransit times and their uncertainties. For convenience, this table also includes the new occultation times described below, as well as the previously reported times that are analyzed in Section 4. The results for the other transit parameters were consistent with the previous results of Maciejewski et al. (2013), though with larger uncertainties.

Time-correlated noise is evident in some of the new light curves. Although we made no special allowance for these correlations in our analysis, we have reason to believe that the quoted uncertainties are reliable. When these seven new midtransit times are fitted with a linear function of epoch, we obtain $\chi^2_{\mathrm{min}} = 5.1$ with five degrees of freedom. When the period is held fixed at the value derived from all 10 years of timing data, we obtain $\chi^2_{\mathrm{min}} = 7.8$ with six degrees of freedom. These tests suggest that the uncertainties are not substantially underestimated. Furthermore, spurious timing variations would be random from night to night, whereas our long-term timing analysis (Section 4) reveals that all seven new midtransit times produce residuals of the same sign and amplitude.

[6] For this purpose we used the online code of Eastman et al. (2013): http://astroutils.astronomy.ohio-state.edu/exofast/limbdark.shtml.

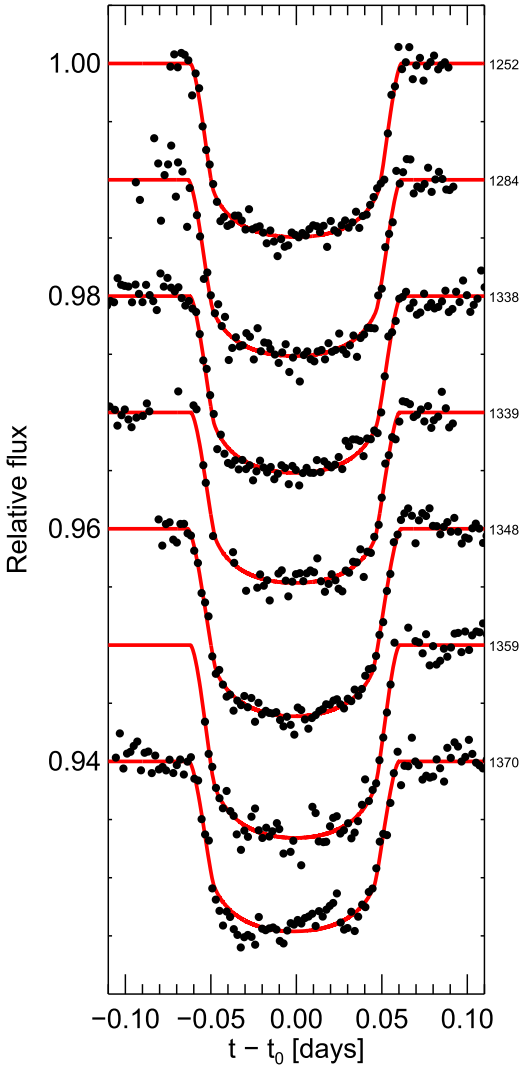

Figure 1. New transit light curves. Black points are based on observations with the FLWO 1.2 m telescope in the Sloan r' band. Red curves are the best-fit models. Epoch numbers are printed to the right of each curve. Vertical offsets have been applied to separate the light curves.

3. New Occultation Times

We measured two new occultation times based on hitherto unpublished *Spitzer* observations in 2013 December (program 90186, P.I. Todorov). Two different transits were observed, one at 3.6 μm and one at 4.5 μm. The data take the form of a time series of 32 × 32-pixel subarray images, with an exposure time of 2.0 s per image. The data were acquired over a wide range of orbital phases, but for our purpose, we analyzed only the ≈14,000 images within 4 hr of each occultation. We also re-analyzed the *Spitzer* occultation presented by Deming et al. (2015) using the technique described below.

We determined the background level in each image by fitting a Gaussian function to the histogram of pixel values, after excluding the high flux values associated with the star. The centroid of the fitted Gaussian function was taken to be the background value and was subtracted from each image prior to performing aperture photometry.

We used two different schemes to choose photometric aperture sizes. In the first scheme, we used 11 apertures ranging in radius from 1.6–3.5 pixels in average increments of

Table 1
Transit and Occultation Times

Type of event	Midpoint (BJD_{TDB})	Uncertainty (days)	Epoch number	
tra	2454515.52496	0.00043	−1640	Hebb et al. (2009)[a]
occ	2454769.28131	0.00080	−1408	Campo et al. (2011)
occ	2454773.64751	0.00060	−1404	Campo et al. (2011)
tra	2454836.40340	0.00028	−1346	Copperwheat et al. (2013)
tra	2454840.76893	0.00062	−1342	Chan et al. (2011)
tra	2455140.90981	0.00042	−1067	Collins et al. (2017)
tra	2455147.45861	0.00043	−1061	Maciejewski et al. (2013)
tra	2455163.83061	0.00032	−1046	Collins et al. (2017)
tra	2455172.56138	0.00036	−1038	Chan et al. (2011)
occ	2455194.93381	0.00100	−1018	Croll et al. (2015)
occ	2455202.57566	0.00220	−1011	Föhring et al. (2013)
tra	2455209.66895	0.00046	−1004	Collins et al. (2017)
tra	2455210.76151	0.00041	−1003	Collins et al. (2017)
tra	2455230.40669	0.00019	−985	Maciejewski et al. (2013)
tra	2455254.41871	0.00043	−963	Maciejewski et al. (2013)
tra	2455494.52999	0.00072	−743	Maciejewski et al. (2013)
tra	2455498.89590	0.00079	−739	Sada et al. (2012)
tra	2455509.80971	0.00037	−729	Collins et al. (2017)
tra	2455510.90218	0.00031	−728	Collins et al. (2017)
occ	2455517.99455	0.00118	−722	Deming et al. (2015)[b]
tra	2455518.54070	0.00040	−721	Cowan et al. (2012)
tra	2455542.55210	0.00040	−699	Cowan et al. (2012)
tra	2455542.55273	0.00028	−699	Maciejewski et al. (2013)
tra	2455566.56385	0.00028	−677	Maciejewski et al. (2013)
occ	2455576.93141	0.00090	−668	Croll et al. (2015)
occ	2455587.84671	0.00170	−658	Croll et al. (2015)
tra	2455590.57561	0.00068	−655	Maciejewski et al. (2013)
tra	2455598.21552	0.00035	−648	Maciejewski et al. (2013)
tra	2455600.39800	0.00029	−646	Maciejewski et al. (2013)
tra	2455601.49010	0.00024	−645	Maciejewski et al. (2013)
tra	2455603.67261	0.00029	−643	Collins et al. (2017)
tra	2455623.31829	0.00039	−625	Maciejewski et al. (2013)
tra	2455876.52786	0.00027	−393	Maciejewski et al. (2013)
tra	2455887.44198	0.00021	−383	Maciejewski et al. (2013)
tra	2455888.53340	0.00027	−382	Maciejewski et al. (2013)
tra	2455890.71635	0.00024	−380	Maciejewski et al. (2013)
tra	2455903.81357	0.00032	−368	Collins et al. (2017)
occ	2455910.90841	0.00130	−362	Crossfield et al. (2012)
tra	2455920.18422	0.00031	−353	Maciejewski et al. (2013)
tra	2455923.45850	0.00022	−350	Maciejewski et al. (2013)
tra	2455924.00411	0.00210	−350	Croll et al. (2015)
tra	2455946.37823	0.00018	−329	Maciejewski et al. (2013)
occ	2455946.92231	0.00180	−329	Croll et al. (2015)
tra	2455947.47015	0.00017	−328	Maciejewski et al. (2013)
tra	2455948.56112	0.00033	−327	Maciejewski et al. (2013)
tra	2455951.83534	0.00011	−324	Stevenson et al. (2014)
tra	2455952.92720	0.00010	−323	Stevenson et al. (2014)
tra	2455959.47543	0.00017	−317	Maciejewski et al. (2013)
tra	2455960.56686	0.00032	−316	Maciejewski et al. (2013)
tra	2455970.38941	0.00039	−307	Maciejewski et al. (2013)
tra	2455971.48111	0.00035	−306	Maciejewski et al. (2013)
tra	2455982.39509	0.00034	−296	Maciejewski et al. (2013)
tra	2455983.48695	0.00035	−295	Maciejewski et al. (2013)
tra	2455984.57797	0.00032	−294	Collins et al. (2017)
tra	2455985.66975	0.00042	−293	Collins et al. (2017)
tra	2455996.58378	0.00037	−283	Collins et al. (2017)
tra	2456005.31533	0.00037	−275	Maciejewski et al. (2013)
tra	2456006.40637	0.00031	−274	Maciejewski et al. (2013)
tra	2456245.42729	0.00033	−55	Maciejewski et al. (2016)
tra	2456249.79404	0.00039	−51	Collins et al. (2017)
tra	2456273.80514	0.00030	−29	Collins et al. (2017)
tra	2456282.53584	0.00030	−21	Maciejewski et al. (2016)
tra	2456284.71857	0.00030	−19	Collins et al. (2017)

Table 1
(Continued)

Type of event	Midpoint (BJD_{TDB})	Uncertainty (days)	Epoch number	
tra	2456297.81605	0.00030	−7	Collins et al. (2017)
tra	2456302.18179	0.00046	−3	Maciejewski et al. (2016)
tra	2456305.45536	0.00024	0	Maciejewski et al. (2016)
tra	2456319.64424	0.00038	13	Collins et al. (2017)
tra	2456328.37556	0.00027	21	Maciejewski et al. (2016)
tra	2456329.46733	0.00029	22	Maciejewski et al. (2016)
tra	2456604.50489	0.00021	274	Maciejewski et al. (2016)
tra	2456605.59624	0.00030	275	Maciejewski et al. (2016)
tra	2456606.68760	0.00033	276	Maciejewski et al. (2016)
tra	2456607.77938	0.00071	277	Collins et al. (2017)
tra	2456629.60726	0.00019	297	Maciejewski et al. (2016)
tra	2456630.69917	0.00043	298	Maciejewski et al. (2016)
occ	2456638.88530	0.00110	305	this work
occ	2456642.15848	0.00141	308	this work
tra	2456654.71047	0.00034	320	Collins et al. (2017)
tra	2456659.07598	0.00034	324	Kreidberg et al. (2015)
tra	2456662.35014	0.00019	327	Maciejewski et al. (2016)
tra	2456663.44136	0.00019	328	Maciejewski et al. (2016)
tra	2456664.53256	0.00031	329	Maciejewski et al. (2016)
tra	2456674.35560	0.00028	338	Kreidberg et al. (2015)
tra	2456677.63039	0.00032	341	Collins et al. (2017)
tra	2456688.54384	0.00040	351	Maciejewski et al. (2016)
tra	2456694.00161	0.00029	356	Kreidberg et al. (2015)
tra	2456703.82417	0.00029	365	Kreidberg et al. (2015)
tra	2456711.46415	0.00025	372	Maciejewski et al. (2016)
tra	2456719.10428	0.00034	379	Kreidberg et al. (2015)
tra	2456721.28692	0.00034	381	Kreidberg et al. (2015)
tra	2456722.37807	0.00046	382	Maciejewski et al. (2016)
tra	2456986.50195	0.00043	624	Maciejewski et al. (2016)
tra	2457010.51298	0.00039	646	Maciejewski et al. (2016)
tra	2457012.69617	0.00049	648	Collins et al. (2017)
tra	2457045.43831	0.00046	678	Maciejewski et al. (2016)
tra	2457046.53019	0.00049	679	Maciejewski et al. (2016)
tra	2457059.62713	0.00035	691	Collins et al. (2017)
tra	2457060.71839	0.00036	692	Collins et al. (2017)
tra	2457067.26715	0.00022	698	Maciejewski et al. (2016)
tra	2457068.35834	0.00020	699	Maciejewski et al. (2016)
tra	2457103.28423	0.00031	731	Maciejewski et al. (2016)
tra	2457345.57867	0.00042	953	Maciejewski et al. (2016)
tra	2457390.32708	0.00033	994	Maciejewski et al. (2016)
tra	2457391.41818	0.00033	995	Maciejewski et al. (2016)
tra	2457426.34324	0.00055	1027	Maciejewski et al. (2016)
tra	2457427.43496	0.00023	1028	Maciejewski et al. (2016)
tra	2457671.91324	0.00035	1252	this work
tra	2457706.83791	0.00037	1284	this work
tra	2457765.77515	0.00028	1338	this work
tra	2457766.86633	0.00039	1339	this work
tra	2457776.68869	0.00029	1348	this work
tra	2457788.69464	0.00048	1359	this work
tra	2457800.69978	0.00032	1370	this work

Notes.
[a] Refers to the light curve obtained by Hebb et al. (2009) with the 2 m Liverpool telescope, as analyzed by Maciejewski et al. (2013).
[b] Re-analyzed in this work.

0.2 pixel. In the second scheme, we tried 11 apertures for which the radius was allowed to vary at each time step, based on the procedure described in Appendix A of Lewis et al. (2013). In this procedure, the aperture radius is taken to be the sum of a constant (ranging from 0–2 pixels) and the noise pixel radius, defined as the square root of the ratio of the square of the total flux integrated over all pixels and the sum of squared-fluxes of individual pixels. The noise pixel radius is specific to each image and allows for possible changes in the shape of the pixel response function with position. We also tried two different methods to choose the center of the apertures: fitting a two-dimensional Gaussian function to the stellar image, and computing the flux-weighted center-of-light. Hence, there were four versions of the photometry: constant versus variable aperture radii, and Gaussian

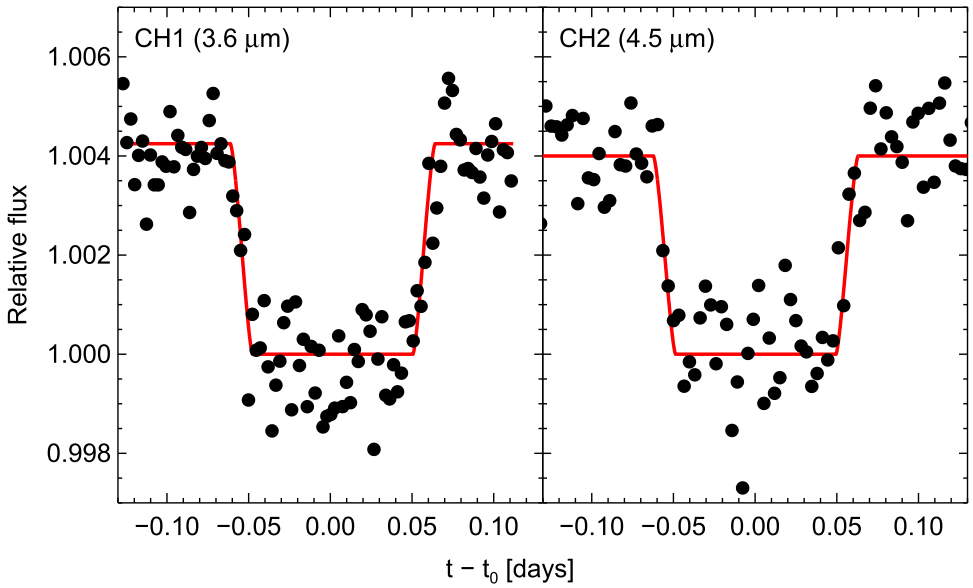

Figure 2. New occultation light curves. Black points are the binned *Spitzer* measurements from epochs 305 (left) and 308 (right). Red curves are the best-fit models.

centroiding versus center-of-light. Each of those four versions contains 11 time series with different aperture sizes.

We corrected for the well-known intrapixel sensitivity variations using pixel-level decorrelation (PLD; Deming et al. 2015). In PLD, the flux time series is modeled as the sum of the astrophysical variation, a temporal baseline, and a weighted sum of the (normalized) time series of each pixel comprising the point-spread function. Because each pixel value is divided by the total brightness of the star in that image, PLD effectively separates astrophysical information and *Spitzer* detector effects. PLD has also been used to produce high-quality photometry from *K2* data (Luger et al. 2016).

Our implementation of PLD operates on time-binned data (see Section 3.1 of Deming et al. 2015). Over a trial range of occultation midpoints and median aperture radii, the code uses linear regression to find the best-fitting occultation depth and pixel coefficients. We provisionally adopt the midpoint that produces the best fit (smallest χ^2). The code then varies the aperture radius from among the 11 possible values and the duration of the time bins. The optimal values of the radius and bin size are determined by examining the Allan (1966) deviation relation of the residuals and identifying the case that comes closest to the ideal relation.[7] Then, an MCMC procedure is used to optimize the light-curve parameters (including the time of mid-occultation), pixel coefficients, and temporal baseline coefficients. The temporal baseline was taken to be a quadratic function of time, which was sufficient to describe the phase-curve variation in the vicinity of the occultation.

After performing these steps for all four different versions of the photometry, we adopted the version that came closest to achieving the theoretical photon noise limit. For the 3.6 μm data, the adopted version used 10-frame binning, center-of-light centroiding, and a constant aperture radius of 2.3 pixels. For the 4.5 μm data, the adopted version used 10-frame binning, center-of-light centroiding, and a constant aperture radius of 2.2 pixels. With these choices, we achieved a noise level of 1.29 and 1.24 times the theoretical photon noise limit at 3.6 and 4.5 μm, respectively. The uncertainty in the midpoint of each occultation was determined from the standard deviation of the (very nearly Gaussian) marginalized posterior distribution. The new light curves are shown in Figure 2, and the times are given in Table 1. The best-fit central times are relatively insensitive to the version of the photometry adopted in the final solution. The very worst of the four photometry solutions for the 3.6 and 4.5 μm data gave midpoints differing by 31 and 75 s (0.3σ and 0.6σ), respectively.

[7] The Allan deviation relation expresses how the standard deviation of the binned residuals varies with bin size. For ideal white noise, it should decrease as the inverse square root of the bin size.

4. Timing Analysis

Table 1 gathers together all of the times of transits ($t_{\rm tra}$) and occultations ($t_{\rm occ}$) used in our analysis. We included all of the data we could find in the literature for which (i) the analysis was based on observations of a single event, (ii) the midpoint was allowed to be a completely free parameter, and (iii) the time system is documented clearly. The tabulated occultation times have not been corrected for the light-travel time across the diameter of the orbit. For the timing analysis described below, the occultation times were corrected by subtracting $2a/c = 22.9$ s.

We fitted three models to the timing data using the MCMC method. The first model assumes a circular orbit and a constant orbital period:

$$t_{\rm tra}(E) = t_0 + PE, \tag{2}$$

$$t_{\rm occ}(E) = t_0 + \frac{P}{2} + PE, \tag{3}$$

where E is the epoch number. Figure 3 displays the residuals with respect to this model. The fit is poor, with $\chi^2_{\rm min} = 197.6$ and 111 degrees of freedom. The transit residuals follow a negative parabolic trend, indicating a negative period derivative. Our new data—the square points at the rightmost extreme of the plot—follow the trend that had been established by Maciejewski et al. (2016). Thus, we confirm the finding of Maciejewski et al. (2016) that the transit interval is slowly shrinking.

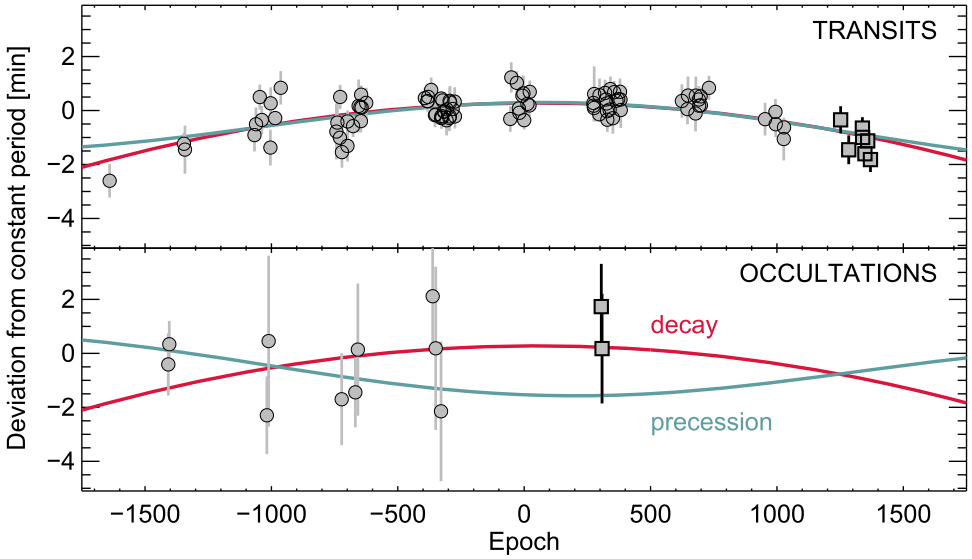

Figure 3. Timing residuals for WASP-12. Each data point is the difference between an observed eclipse time and the prediction of the best-fit constant-period model. The top panel shows transit data and the bottom panel shows occultation data. Circles are previously reported data, and squares are new data. The blue curves show the best-fit precession model, for which transit and occultation deviations are anticorrelated. The red curves show the best-fit orbital decay model, in which the transit and occultation deviations are the same.

Next, we fitted a model that assumes a circular orbit and a constant period derivative:

$$t_{\rm tra}(E) = t_0 + PE + \frac{1}{2}\frac{dP}{dE}E^2, \tag{4}$$

$$t_{\rm occ}(E) = t_0 + \frac{P}{2} + PE + \frac{1}{2}\frac{dP}{dE}E^2. \tag{5}$$

The red curves in Figure 3 shows the best fit, which has $\chi^2_{\rm min} = 118.5$ and 110 degrees of freedom. Both the transit and occultation data are compatible with the model. The implied period derivative is

$$\frac{dP}{dt} = \frac{1}{P}\frac{dP}{dE} = -(9.3 \pm 1.1) \times 10^{-10} = -29 \pm 3 \text{ ms yr}^{-1}. \tag{6}$$

In the third model, the orbit is slightly eccentric and undergoing apsidal precession:

$$t_{\rm tra}(E) = t_0 + P_{\rm s}E - \frac{eP_{\rm a}}{\pi}\cos\omega, \tag{7}$$

$$t_{\rm occ}(E) = t_0 + \frac{P_{\rm a}}{2} + P_{\rm s}E + \frac{eP_{\rm a}}{\pi}\cos\omega, \tag{8}$$

where e is the eccentricity, ω is the argument of pericenter, $P_{\rm a}$ is the anomalistic period and $P_{\rm s}$ is the sidereal period. The argument of pericenter advances uniformly in time,

$$\omega(E) = \omega_0 + \frac{d\omega}{dE}E, \tag{9}$$

and the two periods are related by

$$P_{\rm s} = P_{\rm a}\left(1 - \frac{d\omega/dE}{2\pi}\right). \tag{10}$$

These expressions are based on Equation (15) of Giménez & Bastero (1995), in the limit of low eccentricity and high inclination. This model has five parameters: t_0, $P_{\rm s}$, e, ω_0, and $d\omega/dE$.

The blue curves in Figure 3 show the best-fit precession model. The main difference between the decay and precession models is that apsidal precession produces anticorrelated transit and occultation timing deviations, while the orbital decay model produces deviations of the same sign. The precession fit has $\chi^2_{\rm min} = 124.0$ and 108 degrees of freedom. The model achieves a reasonable fit by adjusting the precession period to be longer than the observing interval. In this way, the parabolic trend can be matched by the downward-curving portion of a sinusoidal function. However, there is tension between the need for enough downward curvature in the transit deviations to fit the earliest data and a small enough upward curvature in the occultation deviations to fit the most recent data.

The orbital decay model provides the best fit. It is better than the precession model by $\Delta\chi^2 = 5.5$, despite the handicap of having two fewer free parameters. The Akaike Information Criterion (AIC) and Bayesian Information Criterion (BIC) are widely used statistics to choose the most parsimonious model that fits the data:

$$\alpha = \text{AIC} = \chi^2 + 2k, \tag{11}$$

$$\beta = \text{BIC} = \chi^2 + k\log n, \tag{12}$$

where n is the number of data points and k is the number of free parameters. In this case, $n = 113$, $k = 3$ for decay, and $k = 5$ for precession. The AIC favors the decay model by $\Delta\alpha = 9.46$, corresponding to a likelihood ratio of $\exp(\Delta\alpha/2) = 113$. The BIC favors the orbital decay model by $\Delta\beta = 14.91$, corresponding to an approximate Bayes factor of $\exp(\Delta\beta/2) = 1730$.

Table 2 gives the best-fit parameters for all three models. In summary, a constant period has been firmly ruled out, and orbital decay is statistically favored over apsidal precession as the best explanation for the timing data. However, the statistical significance of the preference for orbital decay is modest and depends on the reliability of the quoted uncertainties for all of

Table 2
Best-fit Model Parameters

Parameter	Value (Unc.)[a]
Constant period	
Reference epoch, t_0 [BJD_{TBD}]	2456305.455609(28)
Period, P [days]	1.091420025(47)
Orbital decay	
Reference epoch, t_0 [BJD_{TBD}]	2456305.455790(35)
Period at reference epoch, P [days]	1.091420078(47)
dP/dE [days]	$-1.02(11) \times 10^{-9}$
Apsidal precession	
Reference epoch, t_0 [BJD_{TBD}]	2456305.45509(15)
Sidereal period, P_{sid} [days]	1.09141993(15)
Eccentricity, e	0.00208(47)
A.O.P. at reference epoch, ω_0 [rad]	2.92(19)
Precession rate, $d\omega/dE$ [rad epoch^{-1}]	0.00133(18)

Note.
[a] The numbers in parenthesis give the 1σ uncertainty in the final two digits.

the timing data, which come from different investigators using different methods. For example, when the earliest data point is omitted, orbital decay is still preferred but $\Delta\chi^2$ is reduced to 2.0. For these reasons, and out of general caution, we do not regard apsidal precession as being definitively ruled out. Further observations are needed.

5. Implications

5.1. Orbital Decay

To explore the implications of the best-fit models, we assume, for the moment, that the orbital decay interpretation is correct. Based on the current decay rate, the period would shrink to zero in

$$\frac{P}{dP/dt} = 3.2 \text{ Myr}. \tag{13}$$

The future lifetime of the planet is likely to be even shorter, because the decay rate is expected to increase rapidly with decreasing period.

In the simplified "constant phase lag" model for tidal evolution, the period derivative is

$$\frac{dP}{dt} = -\frac{27\pi}{2Q_\star}\left(\frac{M_p}{M_\star}\right)\left(\frac{R_\star}{a}\right)^5, \tag{14}$$

which we obtained by applying *Kepler*'s third law to Equation (20) of Goldreich & Soter (1966). Here, $Q_\star$ is the "modified quality factor" of the star's tidal oscillations (often designated elsewhere as $Q'_\star$). For the case of WASP-12, $M_p/M_\star = 9.9 \times 10^{-4}$ and $a/R_\star = 3.097$ (Chan et al. 2011), giving

$$Q_\star \approx 2 \times 10^5. \tag{15}$$

This value for $Q_\star$ is smaller than the typical range of 10^{6-7} that has been inferred through ensemble analyses of binary stars and star-planet systems (see, e.g., Meibom & Mathieu 2005; Hansen 2010; Penev et al. 2012). One exception is Jackson et al. (2008), who found $Q_\star \sim 10^{5.5}$ based on the period-eccentricity distribution of hot Jupiters. This is consistent with our result.

Theoretically, the quality factor should depend on the orbital period, perturbation strength, and internal structure of the star (Ogilvie 2014). Recently, Essick & Weinberg (2016) calculated $Q_\star$ for hot Jupiters perturbing solar-type stars, based on the nonlinear interactions and dissipation of tidally driven g-modes. For the mass ratio and period of WASP-12, their Equation (26) predicts $Q_\star = 4 \times 10^5$, close to the observed value. However, their calculation pertained to stars with a radiative core and a convective envelope, and it is not clear that WASP-12 belongs in this category. With $T_{eff} = 6100$ K (Torres et al. 2012), WASP-12 is right on the borderline between stars with convective and radiative envelopes. In fact, we wonder if this coincidence—lying right on the Kraft break—could be related to the apparently rapid dissipation rate. The star may have a convective core and a convective envelope, separated by a radiative zone, perhaps leading to novel mechanisms for wave dissipation.

5.2. Apsidal Precession

Assuming instead that the apsidal precession model is correct, the orbital eccentricity is 0.0021 ± 0.0005. This is compatible with the upper limit of 0.05 from observations of the spectroscopic orbit (Husnoo et al. 2012). The observed precession rate is $\dot{\omega} = 26 \pm 3$ deg yr^{-1}, corresponding to a precession period of 14 ± 2 years.

Ragozzine & Wolf (2009) showed that for systems resembling WASP-12, the largest contribution to the theoretical apsidal precession rate is from the planet's tidal deformation. The rate is proportional to the planet's Love number k_p, a dimensionless measure of the degree of central concentration of the planet's density distribution. Lower values of k_p correspond to more centrally concentrated distributions, which are closer to the point-mass approximation and, therefore, produce slower precession. Equation (14) of Ragozzine & Wolf (2009) can be rewritten for this case as

$$\frac{d\omega}{dE} = 15\pi k_p\left(\frac{M_\star}{M_p}\right)\left(\frac{R_p}{a}\right)^5. \tag{16}$$

Using the measured precession rate and relevant parameters of WASP-12, this equation gives $k_p = 0.44 \pm 0.10$. If this interpretation is confirmed, it would be a unique constraint on an exoplanet's interior structure, in addition to the usual measurements of mass, radius, and mean density. For Jupiter, a value of $k_p = 0.59$ has been inferred from its observed gravity moments (Wahl et al. 2016). Therefore, the precession interpretation for WASP-12b suggests that its density distribution has a similar degree of central concentration as Jupiter, and perhaps somewhat higher.

5.3. Prior Probabilities

It is worth contemplating the "prior probability" of each model. By this, we mean the chance that the circumstances required by each model would actually occur, independently of the goodness-of-fit to the data. At face value, both models imply that we are observing WASP-12 at a special time, in violation of the "temporal Copernican principle" articulated by Gott (1993). It is difficult, however, to decide which model requires the greater coincidence.

Given the star's main-sequence age of 1700 ± 800 Myr (Chan et al. 2011), the orbital decay model would have us

believe we are witnessing the last ∼0.2% of the planet's life. If we observed a single system at a random time, this would require a one-in-500 coincidence. However, WASP-12 is not the only hot Jupiter that we and others have been monitoring. There are about 10 other good candidates with comparably low $a/R_\star$, increasing the odds of the coincidence by an order of magnitude.

It is noteworthy that other investigators have argued on independent grounds that WASP-12b is close to death. Fossati et al. (2010), Haswell et al. (2012), and Nichols et al. (2015) have presented near-ultraviolet transit spectroscopy consistent with an extended and escaping exosphere. The resulting mass loss process has been studied theoretically by Li et al. (2010), Lai et al. (2010), and Bisikalo et al. (2013). Most recently, Jackson et al. (2017) developed a new theory for Roche lobe overflow and identified WASP-12 as a likely case of rapid mass loss.

It is also possible that orbital decay occurs in fits and starts, because of strong and erratic variations in the dissipation rate with the forcing period (see, e.g., Ogilvie & Lin 2007; Barker & Ogilvie 2010). Thus, the planet may be experiencing a brief interval of rapid decay. This does not eliminate the requirement for a coincidence, because one would expect to discover the system in one of the more prolonged states of slow dissipation. However, it does mean that the planet's future lifetime may be longer than the current value of $P/\dot{P}$.

As for apsidal precession, the trouble is the very short expected timescale for tidal orbital circularization. This process is thought to be dominated by dissipation within the planet, rather than the star. Equation (25) of Goldreich & Soter (1966), relevant to this case, can be rewritten

$$\tau_e = \frac{e}{|de/dt|} = \frac{2Q_\mathrm{p}}{63\pi}\left(\frac{M_\mathrm{p}}{M_\star}\right)\left(\frac{a}{R_\mathrm{p}}\right)^5 P_\mathrm{orb}. \quad (17)$$

For WASP-12, this gives $\tau_e \sim 0.5$ Myr, assuming $Q_\mathrm{p} \sim 10^6$. At this rate, even 4 Myr of tidal evolution would reduce the eccentricity below 10^{-3}. Of course, the planetary quality factor Q_p could be larger than the standard value of 10^6, or the tidal model leading to the preceding equation could be a gross misrepresentation of the actual circularization process.

There may also be some process that continually excites the eccentricity. One possibility is gravitational forcing by another planet, although no other nearby planets are known in the WASP-12 system (Knutson et al. 2014). An intriguing possibility is eccentricity excitation by the gravitational perturbations from the star's convective eddies. In this scenario, proposed by Phinney (1992) to explain the small but nonzero eccentricities of pulsars orbiting white dwarfs, the system reaches a state of equipartition between the energy of eccentricity oscillations (epicyclic motion) and the kinetic energy of turbulent convection. To our knowledge, this theory has only been developed for post-main-sequence stars (see, e.g., Verbunt & Phinney 1995; Rafikov 2016). It is not obvious that this theory would apply to WASP-12 and be compatible with $e \sim 10^{-3}$.

Should further theoretical investigations reveal that this mechanism (or any other) could naturally maintain the orbital eccentricity at the level of 10^{-3}, then the apsidal precession model would require no special coincidence. Neither would it require unique circumstances; it is possible that eccentricities of this order could exist in other hot Jupiter systems and have remained undetected. Thus, the identification of a natural eccentricity-excitation mechanism would swing the prior-probability balance in the direction of apsidal precession.

5.4. Other Possible Explanations

To this point, we have presented orbital decay and apsidal precession as the only possible reasons for an apparent period decrease. Another possibility is that the star is accelerating toward Earth, due to the force from stellar companions or wide-orbiting planets. This would produce a negative apparent period derivative of $\dot{v}_\mathrm{r}P/c$, where v_r is the radial velocity. Based on long-term Doppler monitoring, Knutson et al. (2014) placed an upper limit for WASP-12 of $|\dot{v}_\mathrm{r}| < 0.019$ m s^{-1} day^{-1} (2σ), which, in turn, limits the apparent $\dot{P}$ to be smaller than 7×10^{-11}. This is an order of magnitude too small to be responsible for the observed period derivative. Of course, none of these phenomena are mutually exclusive. The system may be experiencing a combination of orbital decay, apsidal precession, and radial acceleration, although joint modeling of these effects is not productive with the current data.

Rafikov (2009) described two other phenomena that cause changes in the apparent period of a transiting planet. The first is the Shklovskii effect, wherein the star's proper motion leads to a changing radial velocity and a nonzero second derivative of the light-travel time. This is already ruled out by Doppler observations of the radial acceleration. For completeness, though, we note that the observed distance d and proper motion μ imply a period derivative of $P\mu^2 d/c \sim 6 \times 10^{-15}$, too small to explain the data. The second phenomenon, also dependent on proper motion, is the apparent apsidal precession caused by our changing viewing angle. The resulting period derivative is of order $\sim(P\mu)^2/2\pi$, which in this case is $\sim 10^{-21}$, too small by many orders of magnitude.

6. Future Prospects

With WASP-12, we are fortunate that both possibilities—orbital decay and apsidal precession—lead to interesting outcomes. It will soon be possible to measure the tidal dissipation rate of a star, or the tidal deformability of an exoplanet, either of which would be a unique achievement. To help understand the requirements for a definitive verdict, Figure 4 shows the future projections of a sample of 100 models that provide satisfactory fits to the data, drawn randomly from our converged Markov chains.

For the transits, the two families of models become separated by a few minutes by 2021–22. The occultation models diverge earlier, and are separated by a few minutes in 2019–20. Thus, while continued transit timing is important, the most rapid resolution would probably come from observing occultations a few years from now. In principle, transit duration variations (TDV) would also help to distinguish between the two models, but the expected amplitude is (Pál & Kocsis 2008)

$$\mathrm{TDV} \sim \frac{P}{2\pi}\left(\frac{R_\star}{a}\right) e\cos\omega \sim 10 \text{ sec}, \quad (18)$$

which will be difficult to detect.

In this paper, we have focused on the timing anomalies of WASP-12. This system has other remarkable features we have not even discussed. The star's equator is likely to be misaligned

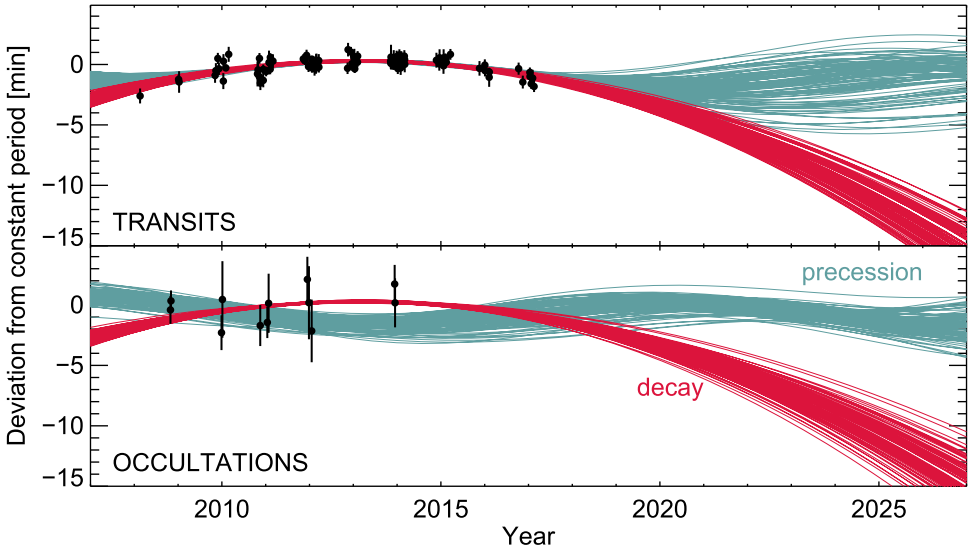

Figure 4. Possible futures for WASP-12. For each of the two models, we randomly drew 100 parameter sets from our Markov chains. Shown here are the extrapolations of those models to future times.

with the orbital plane (Schlaufman 2010; Albrecht et al. 2012). The star is also part of a hierarchical three-body system, with a tight pair of M dwarfs orbiting the planet-hosting star at a distance of about 265 AU (Bechter et al. 2014). Detailed modeling of the star's interior structure and tidal evolution is warranted, as are continued observations of transits and occultations.

We are very grateful to Allyson Bieryla, David Latham, and Emilio Falco for their assistance with the FLWO observations. We thank Nevin Weinberg, Jeremy Goodman, Kaloyen Penev, David Oort Alonso, Heather Knutson, Dong Lai, and the CfA Exoplanet Pizza group for helpful discussions. We also appreciate the anonymous reviewer's prompt and careful report. Work by K.C.P. was supported by the MIT Undergraduate Research Opportunities Program and the Paul E. Gray Fund.

Note added in proof. D. Lai has reminded us of another possible reason for a cyclic variation in period: the Applegate (1992) effect, in which a star's quadrupole moment varies over a magnetic activity cycle. For WASP-12, Watson & Marsh (2010) estimated that this effect could produce timing deviations of 4–40 s depending on the cycle duration. The transit and occultation deviations would have the same sign, allowing this effect to be distinguished from apsidal precession.

References

Albrecht, S., Winn, J. N., Johnson, J. A., et al. 2012, ApJ, 757, 18
Allan, D. W. 1966, IEEEP, 54, 221
Applegate, J. H. 1992, ApJ, 385, 621
Barker, A. J., & Ogilvie, G. I. 2010, MNRAS, 404, 1849
Bechter, E. B., Crepp, J. R., Ngo, H., et al. 2014, ApJ, 788, 2
Bisikalo, D., Kaygorodov, P., Ionov, D., et al. 2013, ApJ, 764, 19
Campo, C. J., Harrington, J., Hardy, R. A., et al. 2011, ApJ, 727, 125
Chan, T., Ingemyr, M., Winn, J. N., et al. 2011, AJ, 141, 179
Claret, A., & Bloemen, S. 2011, A&A, 529, A75
Collins, K. A., Kielkopf, J. F., & Stassun, K. G. 2017, AJ, 153, 78
Copperwheat, C. M., Wheatley, P. J., Southworth, J., et al. 2013, MNRAS, 434, 661
Cowan, N. B., Machalek, P., Croll, B., et al. 2012, ApJ, 747, 82
Croll, B., Albert, L., Jayawardhana, R., et al. 2015, ApJ, 802, 28
Crossfield, I. J. M., Barman, T., Hansen, B. M. S., Tanaka, I., & Kodama, T. 2012, ApJ, 760, 140
Deming, D., Knutson, H., Kammer, J., et al. 2015, ApJ, 805, 132
Eastman, J., Gaudi, B. S., & Agol, E. 2013, PASP, 125, 83
Eastman, J., Siverd, R., & Gaudi, B. S. 2010, PASP, 122, 935
Essick, R., & Weinberg, N. N. 2016, ApJ, 816, 18
Föhring, D., Dhillon, V. S., Madhusudhan, N., et al. 2013, MNRAS, 435, 2268
Foreman-Mackey, D., Hogg, D. W., Lang, D., & Goodman, J. 2013, PASP, 125, 306
Fossati, L., Bagnulo, S., Elmasli, A., et al. 2010, ApJ, 720, 872
Giménez, A., & Bastero, M. 1995, Ap&SS, 226, 99
Goldreich, P., & Soter, S. 1966, Icar, 5, 375
Gott, J. R., III 1993, Natur, 363, 315
Hansen, B. M. S. 2010, ApJ, 723, 285
Haswell, C. A., Fossati, L., Ayres, T., et al. 2012, ApJ, 760, 79
Hebb, L., Collier-Cameron, A., Loeillet, B., et al. 2009, ApJ, 693, 1920
Heyl, J. S., & Gladman, B. J. 2007, MNRAS, 377, 1511
Hoyer, S., Pallé, E., Dragomir, D., & Murgas, F. 2016, AJ, 151, 137
Husnoo, N., Pont, F., Mazeh, T., et al. 2012, MNRAS, 422, 3151
Hut, P. 1980, A&A, 92, 167
Jackson, B., Arras, P., Penev, K., Peacock, S., & Marchant, P. 2017, ApJ, 835, 145
Jackson, B., Greenberg, R., & Barnes, R. 2008, ApJ, 678, 1396
Jordán, A., & Bakos, G. Á 2008, ApJ, 685, 543
Knutson, H. A., Fulton, B. J., Montet, B. T., et al. 2014, ApJ, 785, 126
Kreidberg, L., Line, M. R., Bean, J. L., et al. 2015, ApJ, 814, 66
Lai, D., Helling, C., & van den Heuvel, E. P. J. 2010, ApJ, 721, 923
Levrard, B., Winisdoerffer, C., & Chabrier, G. 2009, ApJL, 692, L9
Lewis, N. K., Knutson, H. A., Showman, A. P., et al. 2013, ApJ, 766, 95
Li, S.-L., Miller, N., Lin, D. N. C., & Fortney, J. J. 2010, Natur, 463, 1054
Luger, R., Agol, E., Kruse, E., et al. 2016, AJ, 152, 100
Maciejewski, G., Dimitrov, D., Fernández, M., et al. 2016, A&A, 588, L6
Maciejewski, G., Dimitrov, D., Seeliger, M., et al. 2013, A&A, 551, A108
Mandel, K., & Agol, E. 2002, ApJL, 580, L171
Matsakos, T., & Königl, A. 2015, ApJL, 809, L20
Mayor, M., & Queloz, D. 1995, Natur, 378, 355
Meibom, S., & Mathieu, R. D. 2005, ApJ, 620, 970
Miralda-Escudé, J. 2002, ApJ, 564, 1019
Nichols, J. D., Wynn, G. A., Goad, M., et al. 2015, ApJ, 803, 9
Ogilvie, G. I. 2014, ARA&A, 52, 171
Ogilvie, G. I., & Lin, D. N. C. 2007, ApJ, 661, 1180
Pál, A., & Kocsis, B. 2008, MNRAS, 389, 191
Penev, K., Hartman, J. D., Bakos, G. Á, et al. 2016, AJ, 152, 127
Penev, K., Jackson, B., Spada, F., & Thom, N. 2012, ApJ, 751, 96
Phinney, E. S. 1992, RSPTA, 341, 39

Rafikov, R. R. 2009, ApJ, 700, 965
Rafikov, R. R. 2016, ApJ, 830, 8
Ragozzine, D., & Wolf, A. S. 2009, ApJ, 698, 1778
Rasio, F. A., Tout, C. A., Lubow, S. H., & Livio, M. 1996, ApJ, 470, 1187
Sada, P. V., Deming, D., Jennings, D. E., et al. 2012, PASP, 124, 212
Sasselov, D. D. 2003, ApJ, 596, 1327
Schlaufman, K. C. 2010, ApJ, 719, 602
Schlaufman, K. C., & Winn, J. N. 2013, ApJ, 772, 143
Stevenson, K. B., Bean, J. L., Seifahrt, A., et al. 2014, AJ, 147, 161
Teitler, S., & Königl, A. 2014, ApJ, 786, 139
Torres, G., Fischer, D. A., Sozzetti, A., et al. 2012, ApJ, 757, 161
Verbunt, F., & Phinney, E. S. 1995, A&A, 296, 709
Villaver, E., & Livio, M. 2009, ApJL, 705, L81
Wahl, S. M., Hubbard, W. B., & Militzer, B. 2016, ApJ, 831, 14
Watson, C. A., & Marsh, T. R. 2010, MNRAS, 405, 2037
Wilkins, A. N., Delrez, L., Barker, A. J., et al. 2017, ApJL, 836, L24
Winn, J. N. 2010, in Exoplanets, Exoplanet Transits and Occultations, ed. S. Seager (Tucson, AZ: Univ. of Arizona Press), 55